Icarus 248 (2015) 539–546

Contents lists available at ScienceDirect

Icarus

journal homepage: www.elsevier.com/locate/icarus

Ionization balance in Titan's nightside ionosphere

E. Vigren [a,f,*], M. Galand [a], R.V. Yelle [b], A. Wellbrock [c], A.J. Coates [c], D. Snowden [b], J. Cui [d], P. Lavvas [e], N.J.T. Edberg [f], O. Shebanits [f], J.-E. Wahlund [f], V. Vuitton [g], K. Mandt [h]

[a] Department of Physics, Imperial College London, London SW7 2AZ, UK
[b] Lunar and Planetary Laboratory, University of Arizona, Tucson 85721-0092, USA
[c] Mullard Space Science Laboratory, University College London, Dorking, Surrey RH5 6NT, UK
[d] Key Laboratory of Lunar and Deep Space Exploration, Chinese Academy of Sciences, Beijing 100012, China
[e] Groupe de Spectrométrie Moléculaire et Atmosphérique, Université Reims Champagne-Ardenne, UMR 7331, 51687 Reims, France
[f] Swedish Institute of Space Physics, Uppsala, Sweden
[g] Univ. Grenoble Alpes, CNRS, IPAG, F-38000 Grenoble, France
[h] Space Science and Engineering Division, Southwest Research Institute, San Antonio, TX 78228, USA

ARTICLE INFO

Article history:
Received 26 March 2014
Revised 27 August 2014
Accepted 7 November 2014
Available online 22 November 2014

Keywords:
Titan
Ionospheres
Titan, atmosphere

ABSTRACT

Based on a multi-instrumental Cassini dataset we make model versus observation comparisons of plasma number densities, $n_P = (n_e n_I)^{1/2}$ (n_e and n_I being the electron number density and total positive ion number density, respectively) and short-lived ion number densities (N^+, CH_2^+, CH_3^+, CH_4^+) in the southern hemisphere of Titan's nightside ionosphere over altitudes ranging from 1100 and 1200 km and from 1100 to 1350 km, respectively. The n_P model assumes photochemical equilibrium, ion–electron pair production driven by magnetospheric electron precipitation and dissociative recombination as the principal plasma neutralization process. The model to derive short-lived-ion number densities assumes photochemical equilibrium for the short-lived ions, primary ion production by electron-impact ionization of N_2 and CH_4 and removal of the short-lived ions through reactions with CH_4. It is shown that the models reasonably reproduce the observations, both with regards to n_P and the number densities of the short-lived ions. This is contrasted by the difficulties in accurately reproducing ion and electron number densities in Titan's sunlit ionosphere.

1. Introduction

Titan, the largest satellite of Saturn, has a dense and extended atmosphere dominated by N_2 and CH_4. The Cassini mission has revealed a chemically complex ionosphere around Titan. N_2 and CH_4 are ionized and/or dissociated by solar photons or particle irradiation marking the onset of a chain of chemical reactions, which produce hydrocarbon and nitrile ions, heavy positive and negative ions, and eventually aerosols (e.g., Vuitton et al., 2007; Coates et al., 2007, 2009; Waite et al., 2007; Wahlund et al., 2009; Crary et al., 2009; Ågren et al., 2012; Shebanits et al., 2013; Lavvas et al., 2013; Wellbrock et al., 2013). However, Titan dayside ionospheric models have shown difficulties in reproducing observed electron number densities (e.g., Vigren et al., 2013), as well as the observed number densities of $HCNH^+$, the dominant ion in the main ionosphere (e.g., Vuitton et al., 2009; Westlake et al., 2012). The sunlit side electron number densities derived in the Cassini multi-instrumental study by Vigren et al. (2013) are systematically a factor of ~2 higher than the values deduced from the Radio Plasma Wave Science/Langmuir Probe (RPWS/LP) measurements. From the latter, the dayside electron number densities are found to peak typically at values ~2000–5000 cm^{-3} in the altitude range 1000–1200 km. The model predicts the observed shape of the electron number density in altitude and both the observations and the model show that a decreased solar zenith angle decreases the altitude and increases the magnitude of the electron number density peak. Whether the cause of the discrepancy in magnitude is overestimated plasma production, underestimated plasma loss or a combination of the two is an open question. There are different levels of agreement in existing model-observation comparisons of short-lived ions in Titan's dayside ionosphere (short-lived ions include e.g., N^+, N_2^+ and CH_x^+ with $x < 5$; ions that are reactive with CH_4 and typically lost in ~5–200 s upon formation in the altitude range 1000–1350 km). On the one hand, Robertson et al. (2009), Westlake et al. (2012) and Richard (2013) obtain a good agreement with the Ion Neutral Mass

* Corresponding author at: Swedish Institute of Space Physics, Box 537, SE-75121 Uppsala, Sweden.
E-mail address: erik.vigren@irfu.se (E. Vigren).

http://dx.doi.org/10.1016/j.icarus.2014.11.012
0019-1035/

Spectrometer/Open Source Ion mode (INMS/OSI) observations for their model derived number densities of $\{N^+,CH_2^+\}$, CH_3^+ and CH_4^+ (note that N^+ and CH_2^+ cannot be separated by the INMS/OSI due to their similar mass-to-charge ratios). On the other hand Vuitton et al. (2009) overestimate the observed number densities of $\{N^+,CH_2^+\}$ and CH_3^+ and Mandt et al. (2012) derive significantly higher number densities than observed for these species as well as for CH_4^+. Nevertheless, when Mandt et al. (2012) utilize a high resolution cross-section set for the N_2 photodissociation beyond the N_2 ionization threshold, an action that affect the ionization rate profile of CH_4 (see Lavvas et al., 2011), the model-data comparison improves notably for CH_3^+ and CH_4^+.

In the present work we focus on Titan's nightside ionosphere with the purpose of comparing modeled ionospheric number densities with observations. Firstly (in Section 2) we compare modeled *plasma number densities* with RPWS/LP observations in the altitude range 1100–1200 km (the selection of upper and lower limits of the altitude range are motivated in Section 2.1). The plasma number density is here defined as $n_P = (n_e n_I)^{1/2}$ with n_e and n_I being the electron number density and the total positive ion number density, respectively. Secondly (in Section 3) we compare over a more extended altitude range (1100–1350 km) modeled and observed number densities of the short-lived ions N^+, CH_2^+, CH_3^+ and CH_4^+.

Titan's nightside ionospheric particle balance has previously been modeled by Ågren et al. (2007) (focusing on the T5 flyby) and Cravens et al. (2009) (focusing on the T5 and T21 flybys). In brief they considered upstream electron fluxes measured by the Cassini Plasma Spectrometer/Electron Spectrometer (CAPS/ELS) and modeled by different means the electron precipitation through the upper atmosphere. The number densities of the dominant N_2 and CH_4 molecules were constrained by measurements by the Ion Neutral Mass Spectrometer (INMS) operating in its Closed Source Neutral (CSN) mode. Ionization rates versus altitude were calculated and electron- and ion number densities derived from ion-chemistry models. In the deep ionosphere, below 1200 km, the modeled electron number densities significantly exceeded the RPWS/LP observations. In Ågren et al. (2007) the modeled n_e exceeded the observations by more than a factor of 6 (see their Fig. 8), though sub-sequent to their work a re-calibration of the CAPS/ELS instrument was made (see Cravens et al., 2009 and in particular Lewis et al., 2010), which taken into account reduces the discrepancy to a factor of ~3. Cravens et al. (2009) remarked that a satisfactory model-observation comparison in the deep ionosphere would be achieved following a reduction by a factor of 5–10 in the incident electron fluxes used in their model.

Our approach to investigate Titan's nightside ionosphere differ in several aspects from the works by Ågren et al. (2007) and Cravens et al. (2009). Most importantly we do not attempt to model the magnetospheric electron precipitation but use instead in each considered location the *ambient* suprathermal electron fluxes measured by the CAPS/ELS to derive electron-impact ionization rates. As highlighted in e.g., Ågren et al. (2007), Cravens et al. (2009), Gronoff et al. (2009) and Snowden et al. (2013) the electron precipitation is highly sensitive to the magnetic field line topology, which in the case of Titan can be very complicated. In fact, Snowden et al. (2013) discuss the results of Ågren et al. (2007) and Cravens et al. (2009) and show that the significant electron flux depletion required to reach consistency with observations in the deep nightside ionosphere is fully plausible. A further difference in our model to derive plasma number densities is that we utilize the concept of an effective ion–electron recombination coefficient, which removes the computational burden of modeling in detail the complex chemistry associated with Titan's ionosphere. We use in the present study the most recently analyzed data from the INMS/CSN (Cui et al., 2012), INMS/OSI (Mandt et al., 2012), CAPS/ELS (see e.g., Lewis et al., 2010; Wellbrock et al., 2012) and RPWS/LP (Edberg et al., 2013; Shebanits et al., 2013).

2. Plasma number density

2.1. Flyby information and description of model

We focus the n_P study to the altitude regime 1100–1200 km using Cassini data from the five consecutive T55–T59 Titan flybys, which share similar geometrical features (see Table 1).

The upper and lower limits of the altitude range are set respectively to probe a photochemically controlled region and a region where magnetospheric electron precipitation is the dominant ionization source on the nightside (see e.g., Robertson et al., 2009; Galand et al., 2014). Overall the study is restricted to nine points sampled from the flybys, mainly because the RPWS/LP made sweep mode measurements only once every 24 s and as we consider only parts of the flybys at sufficiently high solar zenith angles (>110°) such that we can safely neglect any contribution to the ion–electron pair production by solar EUV photons.

Let n_e, n_I and n_N be the number densities of electrons, positive ions and negative ions, respectively. Under the assumptions of photochemical equilibrium, and overall charge neutrality with singly charged positive and negative ions ($n_I = n_e + n_N$) the following ionospheric relation can be derived (see Larsen et al., 1972):

$$P_e = \alpha_{eff} n_e n_I + \alpha_{MN} n_N n_I \quad (1)$$

where α_{eff} and α_{MN} are the effective ion–electron dissociative recombination and ion–ion mutual neutralization rate coefficients, respectively. Introducing $\lambda = n_N/n_e$ and the plasma number density $n_P = (n_e n_I)^{0.5}$ Eq. (1) can be rewritten as

$$P_e = (\alpha_{eff} + \lambda \alpha_{MN}) n_P^2 \quad (2)$$

In the considered altitude regime $n_e > n_N$ (Shebanits et al., 2013) and in addition it is anticipated that $\alpha_{eff} \gg \alpha_{MN}$ (see Vigren et al., 2014). This implies that ion–electron recombination is the dominant plasma neutralization process in the considered altitude range. Assuming further that the effective recombination coefficient is proportional to $(T_e/300)^{-0.7}$ where T_e is the electron temperature (see further Section 2.6.3) Eq. (2) can be reduced to:

$$n_{P,Model} \approx \sqrt{\frac{P_e}{\alpha_{eff,300}(T_e/300)^{-0.7}}} \quad (3)$$

Table 1
Titan nightside flybys considered in the present study with information on date and Saturn Local Time (SLT). Also shown are the values of the Local Time (LT) on Titan, Solar Zenith Angle (SZA), the latitude and the longitude for altitudes of 1200 km along the Cassini inbound trajectory. The values within brackets are those at 1200 km for the outbound part of the flybys.

Flyby (date)	SLT (h)	LT (h)	SZA (°)	Latitude (°)	Longitude (°)
T55 (2009-05-21)	21.95	22.6 [21.0]	159 [122]	4S [39S]	167 [192]
T56 (2009-06-06)	21.91	22.6 [20.7]	154 [115]	14S [49S]	167 [195]
T57 (2009-06-22)	21.87	22.6 [20.3]	149 [107]	23S [59S]	166 [200]
T58 (2009-07-08)	21.83	22.6 [19.7]	141 [99]	33S [68S]	165 [208]
T59 (2009-07-24)	21.78	22.7 [18.2]	134 [91]	43S [75S]	163 [230]

where $n_P = (n_e n_I)^{1/2}$, P_e is the ion–electron pair production rate, T_e is the electron temperature and $\alpha_{eff,300}$ is the effective ion–electron recombination coefficient at a reference electron temperature of 300 K. The input parameters P_e, $\alpha_{eff,300}$ and T_e are discussed in Sections 2.2–2.4. In Section 2.5 the ratios, R, of modeled (right-hand-side of Eq. (3)) and observed plasma number densities are presented with estimated random uncertainties. In Section 2.6 we explore how the R-values are affected considering e.g., systematic errors of various input parameters.

2.2. Electron production rate

The ion–electron pair production rate P_e at a given location is calculated as in Galand et al. (2010) from the CAPS/ELS derived differential suprathermal electron fluxes, $I_e(E)$, (unit of $cm^{-2}\ sr^{-1}\ s^{-1}\ eV^{-1}$) (see e.g., Lewis et al., 2010; Wellbrock et al., 2012) assumed to be isotropic in pitch angle and corrected for spacecraft potential, measured by RPWS/LP (typically in the vicinity of −0.5 V for the points considered):

$$P_e = 4\pi \sum_m n_m \int I_e(E)\sigma_m(E)dE \quad (4)$$

where the integral extends from the ionization threshold of neutral species m to 28 keV, which is the upper limit of the CAPS/ELS energy range, n_m is the number density of molecular species m (N_2 or CH_4) (derived from INMS/CSN, see Cui et al., 2012) and $\sigma_m(E)$ is the total electron-impact ionization cross section of m at energy E. The cross sections for N_2 and CH_4 electron-impact ionization are taken from Itikawa (2006) and Liu and Shemansky (2006). To assess I_e we have mainly made use of the CAPS/ELS anode 2 measurements taking the average over four 2s spectra recorded near the altitude of interest. As an example Fig. 1 shows $I_e(E)$ derived in this manner near 1169 km during the ingress of the T56 flyby (the displayed error bars are due to counting statistics). Anodes 3–6, and in particular anodes 4 and 5, pointed in or near the ram direction and detected negative ions (or traces). Anode 2 was chosen out of the remaining four anodes because it is the least affected by spacecraft obscuration, which in particular affect the measurements in anodes 1 and 8 (e.g., Lewis et al., 2008; Arridge et al., 2009).

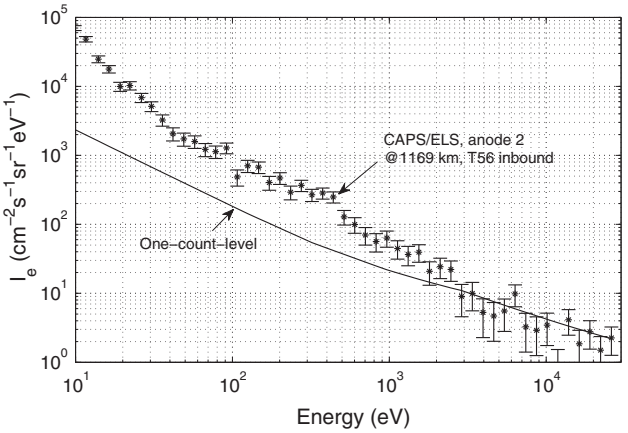

Fig. 1. CAPS/ELS anode 2 derived suprathermal electron intensities versus electron energy for the inbound of the T56 flyby at an altitude of 1169 km. The error bars are due to counting statistics. The displayed data has not been corrected for the spacecraft potential. The solid line shows the level registered by one electron in each energy bin.

In Table 2 for the nine investigated points we list the associated $n(N_2)$, $n(CH_4)$, the calculated ionization frequencies ν_{ioni} of N_2 and CH_4 (based on CAPS/ELS anode 2 derived I_e) and the ion–electron pair production rates, P_e. The random errors due to counting statistics in the INMS/CSN measurements of N_2 number densities are only ~1% (Cui et al., 2012). Accounting for the statistical uncertainties in the suprathermal electron intensities measured by anode 2 of CAPS/ELS give errors in the listed P_e of less than 4% (higher uncertainties for points with lower ionization frequencies). These counting statistic uncertainties combined give random errors in the derived P_e values of less than 5%. We have, however, also considered the CAPS/ELS measurements done with anodes 3, 6 and 7 (the anodes apart from anode 2 that are the least affected by negative ions or spacecraft obscuration effects). The inter-anode variations in $I_e(E)$ resulted in P_e values that in all cases but one (point index 7) were less than 20% different from the P_e values derived using $I_e(E)$ as measured by anode 2. This adds support to our assumption of isotropic electron fluxes. The asymmetric "error margins" in P_e shown in Table 2 correspond to the maximum and minimum values of P_e obtained through calculations based on the $I_e(E)$ measured by anodes 2, 3, 6 and 7 of the CAPS/ELS.

For the ingresses of the T56 and T59 flybys- for which more than one point is given – the ionization frequencies decrease with decreasing altitude (in the case of T56 [T59] by ~30% [~50%] along a decrease in altitude of 45 km). This can be due to various reasons, one possibility being that Titan's atmosphere has degraded in energy impinging magnetospheric electrons at higher altitudes eroding Saturn's flux tubes (Snowden et al., 2013).

2.3. Effective recombination coefficient

The effective ion–electron recombination coefficient at a reference electron temperature of 300 K, $\alpha_{eff,300}$, is defined as the weighted average:

$$\alpha_{eff,300} \equiv \frac{\sum_i n_i \alpha_{i,300}}{\sum_i n_i} \quad (5)$$

where the sums are over individual positive ion species i, n_i is the number density of i and $\alpha_{i,300}$ is the rate coefficient for the dissociative recombination of ion species i at $T_e = 300$ K. The INMS/OSI measurements provide number densities of ions with mass-to-charge ratios M/Z up to 100 Da with unit resolution. To

Table 2
INMS/CSN derived N_2 and CH_4 number densities, calculated ionization frequencies (from anode 2 of CAPS/ELS) and calculated P_e for the nine investigated points in Titan's nightside ionosphere. The asymmetric error margins in the P_e values are based on the maximum and minimum derived P_e when considering the $I_e(E)$ measured by anodes 2, 3, 6 and 7 of the CAPS/ELS (counting statistic errors of the INMS/CSN and CAPS/ELS measurements, affecting P_e by less than 5% are here neglected).

#	Flyby	$n(N_2)$ (10^8 cm^{-3})	$n(CH_4)$ (10^8 cm^{-3})	ν_{ioni} (N_2) (10^{-10} s^{-1})	ν_{ioni} (CH_4) (10^{-10} s^{-1})	P_e (cm^{-3} s^{-1})
1	T55out, 1185 km	4.81	0.37	5.22	7.81	0.28 (+0.00, −0.05)
2	T56in, 1169 km	5.39	0.24	8.14	12.73	0.47 (+0.06, −0.07)
3	T56in, 1124 km	10.39	0.41	5.72	8.77	0.63 (+0.11, −0.11)
4	T56out, 1156 km	4.68	0.32	12.01	17.41	0.62 (+0.06, −0.10)
5	T57in, 1195 km	5.87	0.38	6.03	8.99	0.39 (+0.02, −0.04)
6	T57out, 1147 km	8.38	0.48	4.93	7.40	0.45 (+0.07, −0.03)
7	T58in, 1164 km	6.75	0.35	7.18	11.89	0.53 (+0.00, −0.16)
8	T59in, 1172 km	6.55	0.36	7.72	11.31	0.55 (+0.00, −0.07)
9	T59in, 1127 km	14.76	0.52	4.04	5.75	0.63 (+0.02, −0.01)

relate the M/Z ratios to ion species we use the chemical assignment by Vuitton et al. (2007). We make the assumption that $\alpha_{eff,300}$ is similar to the effective recombination coefficient among the 17 major ions in Titan's nightside ionosphere having masses in the INMS/OSI detectable range (CH_3^+, CH_5^+, $HCNH^+$, $C_2H_5^+$, $CH_2NH_2^+$, c-$C_3H_3^+$, $C_3H_5^+$, CH_3CNH^+, $C_4H_3^+$, $HCCCNH^+$, $C_4H_5^+$, CH_2CHCNH^+, $C_5H_5^+$, $C_4H_3NH^+$, $C_5H_7^+$, $C_6H_7^+$, $C_7H_7^+$). The individual major ion species' recombination coefficients are, when available, taken from laboratory measurements (Adams and Smith, 1988; Rebrion-Rowe et al., 1998; Fournier et al., 2013; Vigren et al., 2013 and references therein). In cases where the dissociative recombination rate coefficient of a major ion species not has been measured (which to the best of our knowledge is the case for $CH_2NH_2^+$, $C_3H_5^+$, $C_5H_5^+$, $C_4H_3NH^+$, $C_5H_7^+$) we set the values according to Eq. (8) of Vigren et al. (2013) which links measured dissociative recombination rate coefficient of $C_xN_yH_z^+$ ion species to the number of atoms within them. For the flybys considered in the study, the INMS/OSI operated only during T57 and T59. This allowed estimations of $\alpha_{eff,300}$ in four out of the nine points considered in the study (see point indices 5, 6, 8 and 9 in Table 3). The $\alpha_{eff,300}$ values for the points associated with the T55, T56 and T58 flybys were instead set based on a linear fit (see Fig. 2) of the $\alpha_{eff,300}$ values calculated against altitude (1100–1200 km) during the T57 and T59 flybys:

$$\alpha_{eff,300}(z) = 1.945 \times 10^{-6} - 1.068 \times 10^{-9} \times z \quad (6)$$

where the altitude z is inserted in km to give $\alpha_{eff,300}$ in $cm^3\ s^{-1}$. All points, with exception for a point near 1100 km during the ingress of the T59 flyby are within 8% of the linear fit, and so we consider an 8% random uncertainty when applying Eq. (6) as an estimate of $\alpha_{eff,300}$ for point indices 1–4 and 7.

It is stressed that additional uncertainties, mainly of systematic nature, prevails for all $\alpha_{eff,300}$ values used in our model calculations. On the one hand, error margins due to uncertainties in the adopted recombination coefficients and the number densities of the 17 major ions are limited to ~15–20% as motivated in Section 2.6.2. It is, on the other hand, difficult to assess the potential error introduced when approximating $\alpha_{eff,300}$ in the entire ion population by the effective recombination coefficient among the 17 major ions observable by the INMS/OSI. While the 17 major ions account for >90% of the ion population seen by the INMS/OSI in the considered altitude range, the prevalence of heavy ions (with M/Z > 100 Da), not detectable by the INMS/OSI, may have a non-negligible influence on the effective recombination coefficient. Such heavy ions are considered likely to contribute to somewhat increasing $\alpha_{eff,300}$ values (see Vigren et al., 2013) though there is a limited knowledge on dissociative recombination rate coefficients for complex ions of potential relevance for Titan's ionosphere.

Table 3
Estimated $\alpha_{eff,300}$ and RPWS/LP derived T_e, n_e and n_I for the nine investigated points in Titan's ionosphere. Random errors in $\alpha_{eff,300}$ are only considered for the values derived from Eq. (6) (see text for details) while the random errors in T_e, n_e and n_I are estimated as 20%, 10% and 10%, respectively.

#	Flyby	$\alpha_{eff,300}$ (10^{-7} $cm^3\ s^{-1}$)	T_e (K)	n_e (cm^{-3})	n_I (cm^{-3})
1	T55out, 1185 km	6.79 ± 0.54	648	706	644
2	T56in, 1169 km	6.97 ± 0.56	729	986	1375
3	T56in, 1124 km	7.45 ± 0.60	440	1000	1405
4	T56out, 1156 km	7.10 ± 0.57	686	908	1527
5	T57in, 1195 km	6.64	641	878	942
6	T57out, 1147 km	7.15	507	957	1135
7	T58in, 1164 km	7.02 ± 0.56	667	1078	1753
8	T59in, 1172 km	7.15	646	935	1132
9	T59in, 1127 km	7.74	562	907	808

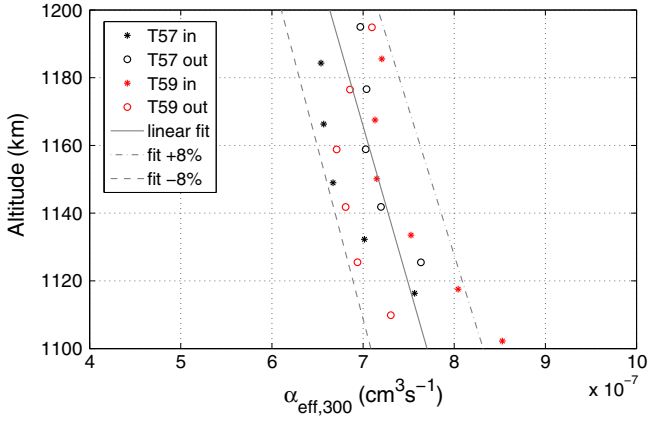

Fig. 2. Effective recombination coefficients at a reference electron temperature of 300 K versus altitude along the Cassini T57 (black) and T59 (red) trajectories. The displayed $\alpha_{eff,300}$ values have been calculated as outlined in Section 2.3 from INMS/OSI ion spectra, chemical assigning and laboratory derived or estimated dissociative recombination rate coefficients of individual ion species. The solid line shows a linear fit of the data (given by Eq. (6)) and the dashed-dotted and dashed lines are located 8% above and below the fit line, respectively. (For interpretation of the references to colour in this figure legend, the reader is referred to the web version of this article.)

2.4. RPWS/LP data

The RPWS/LP derived T_e, n_e and n_I (see Edberg et al., 2011, 2013; Shebanits et al., 2013) are shown in Table 3. The T_e values are estimated accurate to within ~20% while the random uncertainties in n_e and n_I due to instrumental noise are estimated as ~10%.

2.5. Model-observation comparison

The modeled (right-hand-side of Eq. (3)) and observed plasma number densities [$n_P = (n_e n_I)^{1/2}$], and their ratio $R = n_{P,\mathrm{model}}/n_{P,obs}$, are shown in Table 4. The error margins do not take into account systematic uncertainties (discussed in Section 2.6). The assymetric errors in $n_{P,Model}$ and the R-values follows from the asymmetric errors considered for P_e (see Table 2). The error margins include also the consideration of random errors in T_e (20%) and in $\alpha_{eff,300}$ (8% for point indices 1–4 and 7). The random uncertainty in $n_{P,obs}$ follows from error propagation of $n_{P,obs} = (n_e n_I)^{1/2}$ with the random uncertainties in n_e and n_I each set to 10%.

We have plotted the R-values with asterisks in Fig. 3 and included for comparison the corresponding R-values in the dayside ionosphere using Cassini data from the T40 (circles) and T48 Titan flybys (squares). Note that P_e was derived in a different manner in the dayside ionosphere where the main ionization source is photoionization. The central input parameters in the dayside P_e calculations are the solar EUV spectrum impinging on the top of the atmosphere [based on measurements by the Thermosphere Ionosphere Mesosphere Energetic and Dynamics/Solar EUV Experiment, TIMED/SEE (see Woods et al., 2005)] and the INMS/CSN derived number density profiles of N_2 and CH_4. In brief the Beer–Lambert law is applied to derive photoionization rates and generate photoelectron spectra at different locations along the Cassini trajectories, which are then used in an electron-energy degradation model (see Appendix of Vigren et al., 2013) to calculate electron-impact ionization rates. It is seen in Fig. 3 that while the nine nightside points are scattered around $R = 1$ (with the minimum and maximum R values being 0.84 and 1.31, respectively), the 14 dayside points are all associated with R-values of ~1.88 ± 0.12.

Table 4
Modeled and observed n_P and their ratios for the nine investigated points.

#	Flyby	$n_{P,Model}$ (cm^{-3})	$n_{P,observed}$ (cm^{-3})	$R = n_{P,Model}/n_{P,obs}$
1	T55out, 1185 km	841 (+67, −140)	674 ± 48	1.25 (+0.14, −0.24)
2	T56in, 1169 km	1121 (+165, −169)	1164 ± 82	0.96 (+0.17, −0.17)
3	T56in, 1124 km	1052 (+180, −172)	1185 ± 84	0.89 (+0.18, −0.17)
4	T56out, 1156 km	1248 (+164, −196)	1178 ± 83	1.06 (+0.17, −0.20)
5	T57in, 1195 km	1000 (+97, −118)	909 ± 64	1.10 (+0.15, −0.17)
6	T57out, 1147 km	953 (+143, −97)	1042 ± 74	0.91 (+0.18, −0.12)
7	T58in, 1164 km	1149 (+93, −266)	1375 ± 97	0.84 (+0.09, −0.21)
8	T59in, 1172 km	1147 (+80, −150)	1029 ± 73	1.12 (+0.12, −0.19)
9	T59in, 1127 km	1123 (+98, −87)	856 ± 61	1.31 (+0.16, −0.15)

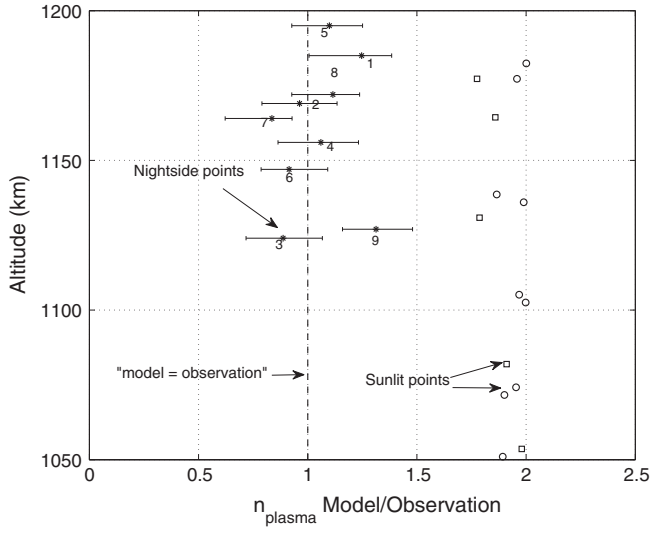

Fig. 3. Modeled divided by observed plasma number densities (R-values) for the nightside points (asterisks with indices of Table 2) and dayside points (open symbols; the circles and squares are for the T40 and T48 flybys, respectively). The asymmetric error bars attached to the nightside points are due to random uncertainties (see text for details). The mean R-value of the displayed sunlit points is 1.92 and the standard deviation of the mean is 0.08.

2.6. Sensitivity tests

2.6.1. Uncertainties in input parameters affecting P_e

As motivated in Vigren et al. (2013) the neutral number densities derived by the INMS/CSN (Cui et al., 2012) are unlikely to be systematically off by more than 20%. The electron-impact ionization cross-sections of N_2 and CH_4 are accurate to within 10% at least for electron energies less than 1 keV (see discussions in Itikawa (2006) and Liu and Shemansky (2006)). In addition to counting statistics uncertainties in the CAPS/ELS anode 2 derived $I_e(E)$, there is also an uncertainty of ∼10% for energies less than 3 keV and ∼20% above 3 keV due to uncertainties in the geometric factor of the instrument (see Lewis et al., 2010). Regarding additional error sources in the CAPS/ELS anode 2 derived $I_e(E)$ it is noted that we have not corrected for (1) uncertainties due to possible local spacecraft obscuration effects on anode 2 data, and (2) RTG background (Arridge et al., 2009). The uncertainties due to these effects are expected to be minor compared to the other dominant uncertainties described above. Errors in P_e associated with uncertainties in the spacecraft potential (which for the considered points are in the range of −0.5 to −1 V according to RPWS/LP measurements) are estimated to be limited to a few percent.

2.6.2. Systematic uncertainties in the $\alpha_{eff,300}$ values

Here we present an attempt to estimate systematic uncertainties in the $\alpha_{eff,300}$ values derived for points in the 1100–1200 km altitude range along the ingress of the T59 flyby. The $\alpha_{eff,300}$ values, shown by red asterisks in Fig. 2, were estimated based on Eq. (5) with summation over the 17 major ions, J, detectable by the INMS/OSI, a chemical assignment of M/Z ratios to ionic species, and measured or "estimated-only" dissociative recombination rate coefficients as described more detailed in Section 2.3. We have made 1000 test simulations (of type S1) with ion number densities, n_J, fixed according to the INMS/OSI measurements during the ingress of the T59 flyby, but with the measured and "estimated only" dissociative recombination coefficients, $\alpha_{J,300}$, being randomly varied within 20% and 50%, respectively. To clarify, for a given S1 simulation the recombination coefficient of species J was given a random value in the interval $[0.8 \times \alpha_{J,300}, 1.2 \times \alpha_{J,300}]$ or $[0.5 \times \alpha_{J,300}, 1.5 \times \alpha_{J,300}]$ depending on whether J has a measured or estimated only recombination coefficient, respectively. To account for 27% error margins in the INMS/OSI derived ion number densities (see Mandt et al., 2012) we have in addition made 1000 simulations (of type S2) in which also the number density of each species J at any given point was given a random value within an interval $[0.73 \times n_J, 1.27 \times n_J]$. The simulation results from S1 and S2 are presented in Table 5.

The modified $\alpha_{eff,300}$ values obtained in the S1 [S2] simulations were changed typically (in 70% of the simulations) by less than 6% [7%] and in the most extreme cases by up to ∼18% [∼22%]. The relative abundance of ions with unmeasured dissociative recombination rate coefficients among the 17 major ions is <20% in the considered altitude range, so considering even larger errors than 50% in the "estimated only" rate coefficients does not affect significantly the results of the test runs. Note, finally, that our consideration of ion number density errors in S2 totally neglects correlation effects; for example it is probably unlikely that the derived number density of $HCNH^+$ (M/Z = 28 Da) is 20% over-determined at the same time as the number density of $C_2H_5^+$ (M/Z = 29 Da) is 20% under-determined. In case all ion number densities are changed by the same factor, and the dissociative recombination rate coefficients are held fixed, there is no change in any given $\alpha_{eff,300}$ value as it is determined as a number density weighted average.

2.6.3. Electron temperature dependence of the effective recombination coefficient

The assumption that the effective recombination coefficient is proportional to $(T_e/300)^{-0.7}$ is backed up by experimental results (see Vuitton et al., 2007; Vigren et al., 2013 and references therein). By instead using a temperature dependence of $(T_e/300)^{-0.5}$ decreases the R-values in Table 4 by a maximum of ∼8%. Similarly a maximum increase of the R-values in Table 4 by ∼9% follows by instead assuming an electron temperature dependence of $(T_e/300)^{-0.9}$.

2.6.4. Considering only the electrons with $E < 1$ keV

We have investigated how the R-values are affected by calculating Eq. (4) only up to ∼1 keV. The sensitivity test is motivated in

Table 5
Results from 1000 simulations of type S1 and 1000 simulations of type S2 applied to the ingress of the T59 flyby. The notation #VW10% should be read as the number of simulations that resulted in effective recombination coefficients within 10% of the $\alpha_{eff,300}$ value displayed in the second column.

Altitude (km)	$\alpha_{eff,300}$ (10^{-7} cm^3 s^{-1})	S1 #VW5%	S1 #VW10%	S1 #VW15%	S2 #VW5%	S2 #VW10%	S2 #VW15%
1186	7.21	566	888	988	479	826	966
1168	7.13	582	893	990	524	875	978
1150	7.15	602	912	993	542	882	983
1134	7.53	632	938	997	591	909	988
1118	8.04	655	947	997	616	917	996
1102	8.53	647	946	996	661	949	995

part by the lack of experimental data of electron-impact ionization cross sections above 1 keV but mainly by the fact that $I_e(E)$ values above 1 keV tend to be highly uncertain due to poor statistics. For seven of the nine points considered the R-values decreased by ~5% while the R-values of point indices 6 and 9 in Table 4 decreased by ~8%.

2.6.5. Electron and positive ion number densities

We have investigated how the R-values are affected by setting n_I equal to the observed electron number densities, the latter being confirmed by an independent measurement technique wherein n_e is determined from the upper hybrid emission line as obtained by the Wideband Receiver on the RPWS (see e.g., Wahlund et al., 2009). This (extreme) test is motivated by the fact that the negative ion number densities inferred from CAPS/ELS measurements (see Wellbrock et al., 2013) in general are lower than the negative ion charge densities inferred from the difference of the RPWS/LP derived n_I and n_e values (Shebanits et al., 2013). While the R-values (i.e. the $n_{P,Model}/n_{P,obs}$ ratios) displayed in Table 4 ranges from 0.84 to 1.31, has a mean of 1.05 and a standard deviation of 0.16, the ratios $n_{P,Model}/n_{e,obs}$ ranges instead from 1.05 to 1.37, has a mean of 1.16 and a standard deviation of 0.12. This shows that the modeled nightside plasma densities are in reasonable agreement with observations, regardless of considering the RPWS/LP derived n_I values or using the assumption that $n_I \sim n_e$.

3. Short-lived ion number densities (T57 case study)

The electron impact production rates of N_2^+, N^+, CH_4^+, CH_3^+ and CH_2^+ can be derived from Eq. (3) applying partial ionization cross sections of N_2 or CH_4. We have taken electron-impact partial ionization cross-sections from Itikawa (2006) and Liu and Shemansky (2006) for N_2 and CH_4, respectively. Fig. 4 shows calculated electron-impact production rates of the five listed ion species versus altitude along the ingress of the T57 trajectory. Across the considered altitude range (1350–1100 km) the production rate of N_2^+ is the highest (71–75% of the total amount of ions formed by electron-impact ionization), followed by N^+ (18–19%), CH_4^+ (5.3–2.7%), CH_3^+ (4.1–2.1%) and CH_2^+ (0.7–0.4%).

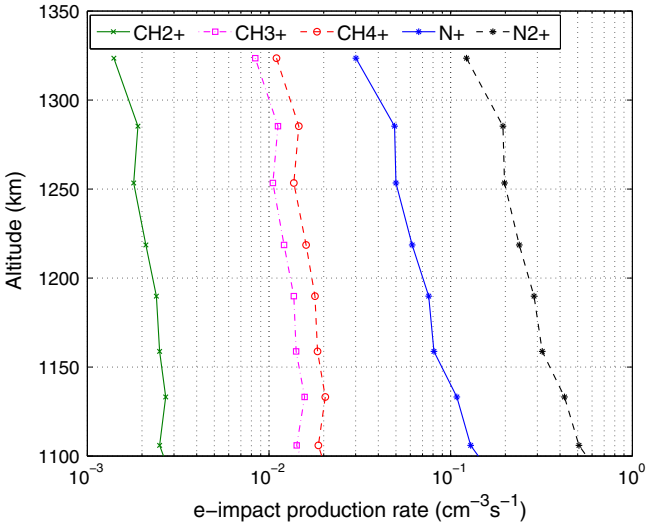

Fig. 4. Calculated production rates of selected ions due to electron impact ionization of N_2 and CH_4 versus altitude along the ingress of the T57 flyby by the Cassini spacecraft.

When focusing on short-lived ions (with significantly shorter lifetimes than species chemically removed primarily through dissociative recombination), the assumption of photochemical equilibrium can be extended to altitudes exceeding 1300 km (see e.g., Robertson et al., 2009; Cui et al., 2009; Cravens et al., 2010). By combining the electron-impact production rates of the ions (shown in Fig. 4) with the rate coefficients for a set of ion-neutral reactions involving CH_4 as the neutral reactant (see Table 6, Dutuit et al., 2013, and the supplementary material of Vuitton et al. (2007)) we have estimated the number densities of {N^+,CH_2^+}, CH_3^+ and CH_4^+ and compared with the INMS/OSI observations (Mandt et al., 2012) of species with M/Z = 14, 15 and 16 Da (see Fig. 5). The modeled N_2^+ number density (less than 10 cm^{-3} in the considered altitude range) could not be compared with INMS/OSI observations as M/Z = 28 Da ions are heavily dominated by $HCNH^+$. The error margins shown in Fig. 5 for the model-derived short-lived ion number densities account for the inter-anode variations in derived electron-impact ion-production rates (CAPS/ELS measurements by anode 2, 3, 6 and 7 were considered) and 20% uncertainties in the rate coefficients used for the ion-neutral reactions. In addition to the displayed error estimates it is noted that the neglect of ion losses via reactions with neutrals other than CH_4 (such as H_2, C_2H_2, C_2H_4 and HCN) is a source of systematic over-determination of ion number densities. This applies in particular for the N^+ ion species, which is reactive with H_2, C_2H_2, C_2H_4 (for rate coefficients, see Dutuit et al., 2013) and with HCN. Considering the number density profiles derived/adopted in earlier Titan models (see e.g., Vuitton et al., 2007; Cravens et al., 2009; Westlake et al.,

Table 6
Ion-neutral reactions considered in the model for calculating number densities of short-lived ions. The notation "Other" means ions other than N_2^+, N^+, CH_4^+, CH_3^+ and CH_2^+. The rate coefficient and branching fractions are adopted from the lists of Vuitton et al. (2007) and Dutuit et al. (2013).

Reaction	Rate coefficient (cm^3 s^{-1})	Produced ion	Branching fraction (%)
$N_2^+ + CH_4$	1.18(−9)[a]	CH_3^+	86
		CH_2^+	9
		Other	5
$N^+ + CH_4$	1.15(−9)	CH_4^+	5
		CH_3^+	50
		Other	45
$CH_4^+ + CH_4$	1.14(−9)	Other	100
$CH_3^+ + CH_4$	1.10(−9)	Other	100
$CH_2^+ + CH_4$	1.30(−9)	Other	100

[a] e.g., 1.18(−9) should be read as 1.18×10^{-9}.

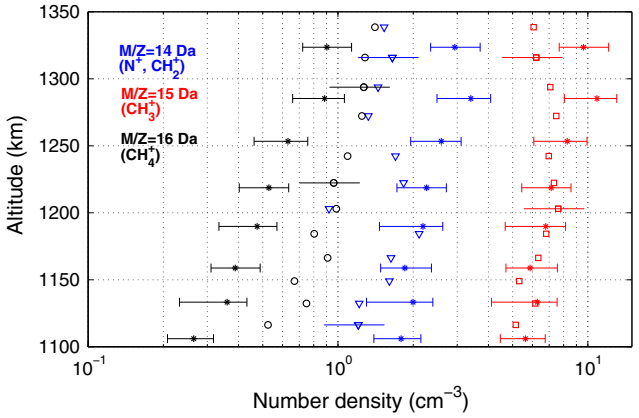

Fig. 5. INMS/OSI observed number densities (open symbols) and calculated number densities (asterisks) of ions with mass to charge ratios of 14 (blue), 15 (red) and 16 (black) Da versus altitude along the ingress of the T57 Titan flyby by the Cassini spacecraft. The 27% error bars associated with the INMS/OSI measurements are for visibility purposes shown only for selected points. The error margins associated with the model-derived number densities account for inter-anode variations in the CAPS/ELS derived ion production rates and 20% uncertainties in the rate coefficients adopted for the ion-neutral reactions. (For interpretation of the references to colour in this figure legend, the reader is referred to the web version of this article.)

2012) – with the number densities of HCN, C_2H_2 and C_2H_4 being at ~1% to a few percent with respect to the number density of CH_4 and with the $n(H_2)/n(CH_4)$ ratio taking values from ~0.1 to ~0.2 in the altitude range 1100–1350 km – we find it reasonable to assume that our model over-determines the N^+ number density by ~20% over the studied altitude range 1100–1350 km. A roughly similar over-determination in CH_2^+ number density is anticipated by neglecting the listed set of neutrals. Thus, our simplification of only consider reactions with CH_4 as the neutral reactant is deemed likely to result in model-derived $\{N^+, CH_2^+\}$ number densities over-determined by up to 20%.

The model derived number densities for ions with M/Z = 14 Da (N^+ and CH_2^+) agree reasonably well with observations for altitudes less than 1250 km (see the blue symbols in Fig. 5). Noteworthy, there is a point near 1200 km in which the observed number density of 14 Da ions deviates markedly from the density profile. Whether this particular discontinuity is real or due to an instrumental artifact remains to be resolved. Near 1300 km the modeled number densities are higher than the observed values by a factor of ~2. The modeled number densities show a decreasing trend with decreasing altitude, which interestingly, is not seen in the observations. Therefore, one may speculate either that transport effects become important above ~1250 km (which seems unlikely considering the short time-scales for the considered ion-neutral reactions) or that there is a missing loss mechanism for N^+ (predicted to contribute to ~73–75% of the signals at M/Z = 14 Da) and that this loss mechanism is dominating more at high altitudes.

The model derived number densities for ions with M/Z = 15 Da (CH_3^+) agree very well with observations again up to an altitude of ~1250 km (see the red symbols in Fig. 5). This validates the ionization frequencies derived from the CAPS/ELS measurements as the dominant source of CH_3^+ is the production through the reaction between N_2^+ and CH_4 and as the N_2^+ production rate by electron-impact is only 20–30% lower than the total electron-impact ionization rate. For the less abundant ions with M/Z = 16 Da (CH_4^+) there is a good agreement in the shapes of the modeled and observed number density profiles (see black symbols in Fig. 5), though the modeled ion number densities are typically 30–40% lower than the observed values. Speculatively the discrepancy may in part be explained by the fact that we do not here consider ions in excited states. For example, N^+ ions in the ^1D state are not quenched by N_2 but react with CH_4 with a similar rate coefficient as ground-state ions, but with a much higher flux (~40% instead of ~5%) into the charge transfer channel, producing CH_4^+ (see Dutuit et al., 2013 and references therein).

4. Discussion and concluding remarks

In summary we have shown that models driven by Cassini data are able to reasonably reproduce both the RPWS/LP derived plasma number densities and the INMS/OSI derived short-lived ion number densities in Titan's nightside ionosphere at least in the altitude ranges 1100–1200 km, and 1100–1250 km, respectively. This is contrasted by the over-estimations in modeled plasma number densities (e.g., Vigren et al., 2013) and short-lived ion number densities (e.g., Mandt et al., 2012) compared with observations in Titan's sunlit ionosphere, where the main ionization source is solar EUV irradiation.

The R-values (i.e. the $n_{P,Model}/n_{P,obs}$ ratios) provided in Table 4 and displayed in Fig. 3 for the nine nightside points considered ranges from 0.84 to 1.31, has a mean of 1.05 and a standard deviation of 0.16. Systematic errors associated with the model input parameters and the observed electron number densities are unlikely to significantly alter (i.e. by a factor of 2 or even a factor of 1.5) the derived nightside R-values (as discussed in Section 2.6). It is, however, important to note that our approach to model the nightside ionosphere is somewhat simplified. For example, the applicability of the photochemical equilibrium assumption needs to be critically evaluated, in particular for modeling n_P on the nightside where the time-scale for loss through dissociative recombination approaches 10^4 s near 1200 km (for long-lived ions such as $HCNH^+$) and where part of the plasma population may be remnant from the dayside (see Cui et al., 2009, 2010). Taking the latter effect into account would act in the direction to increase the modeled plasma number densities, but would not influence the model focusing on short-lived ion number densities.

In the sunlit ionosphere the modeled plasma number densities are higher than the observed values by a factor of ~1.9 (see Fig. 3 and Vigren et al., 2013). The main reason as to why models significantly overestimate n_P in Titan's sunlit ionosphere remains unclear and further studies into the subject are required before conclusions can be drawn.

Acknowledgments

E.V. is grateful for funding from the Swedish Research Council (contract No. 2011-894). M.G. is partially funded by the Science & Technology Facilities Council (STFC) through the consolidated grant to Imperial College London. R.V.Y. acknowledges support of NASA Grant NNX09AB58G. J.C. is supported by the National Science Foundation of China through Grants NFSC-41174146 and 41374178. This work was performed in the framework of the Marie Curie International Research Staff Exchange Scheme PIRSES-GA-2009-247509. Support for this work was provided by a Centre National d'Etudes Spatiales Cassini Participating Scientist grant (to V.V.). N.J.T.E. acknowledges support from the Swedish Research Council and the Swedish National Space Board. The authors thank Chris Arridge for useful comments. AW and AJC acknowledge support from STFC via the UCL-MSSL consolidated grant. Finally, we acknowledge two anonymous reviewers whose comments helped improving the manuscript.

References

Adams, N.G., Smith, D., 1988. Measurements of the dissociative recombination coefficients for several polyatomic ion species at 300 K. Chem. Phys. Lett. 144, 11–14.

Ågren, K., Wahlund, J.-E., Modolo, R., et al., 2007. On magnetospheric electron impact ionisation and dynamics in Titan's ram-side and polar ionosphere – A Cassini case study. Ann. Geophys. 25, 2359–2369.
Ågren, K., Edberg, N.J.T., Wahlund, J.-E., 2012. Detection of negative ions in the deep ionosphere of Titan during the Cassini T70 flyby. Geophys. Res. Lett. 39, L10201.
Arridge, C.S. et al., 2009. The effect of spacecraft radiation sources on electron moments from the Cassini CAPS electron spectrometer. Planet. Space Sci. 57, 854–869.
Coates, A.J., Crary, F.J., Lewis, G.R., et al., 2007. Discovery of heavy negative ions in Titan's ionosphere. Geophys. Res. Lett. 34, L22103.
Coates, A.J., Wellbrock, A., Lewis, G.R., et al., 2009. Heavy negative ions in Titan's ionosphere: altitude and latitude dependence. Planet Space Sci. 57, 1866–1871.
Crary, F.J., Magee, B.A., Mandt, K., Waite Jr., J.H., Westlake, J., Young, D.T., 2009. Heavy ions, temperatures and winds in Titan's ionosphere: Combined Cassini CAPS and INMS observations. Planet. Space Sci. 57, 1847–1856.
Cravens, T.E. et al., 2009. Model-data comparisons for Titan's nightside ionosphere. Icarus 199, 174–188.
Cravens, T.E., Richard, M., Ma, Y.-J., et al., 2010. Dynamical and magnetic field time constants for Titan's ionosphere: Empirical estimates and comparisons with Venus. J. Geophys. Res. 115, A08319.
Cui, J. et al., 2009. Diurnal variations of Titan's ionosphere. J. Geophys. Res. 114, A06310.
Cui, J. et al., 2010. Ion transport in Titan's upper atmosphere. J. Geophys. Res. 115, A06314.
Cui, J. et al., 2012. The CH_4 structure in Titan's upper atmosphere revisited. J. Geophys. Res. 117, E11006.
Dutuit, O. et al., 2013. Critical review of N, N^+, N_2^+, N^{++} and N_2^{++} main production processes and reactions of relevance to Titan's atmosphere. Astrophys. J. Suppl. 204, 20.
Edberg, N.J.T. et al., 2011. Structured ionospheric outflow during the Cassini T55–T59 Titan flybys. Planet. Space Sci. 59, 788–797.
Edberg, N.J.T. et al., 2013. Solar cycle modulation of Titan's ionosphere. J. Geophys. Res. 118, 5255–5264.
Fournier, J.A. et al., 2013. A novel technique for measurement of thermal rate constants and temperature dependences of dissociative recombination: CO_2^+, CF_3^+, N_2O^+, $C_7H_8^+$, $C_7H_7^+$, $C_6H_6^+$, $C_6H_5^+$, $C_5H_6^+$, $C_4H_4^+$, and $C_3H_3^+$. J. Chem. Phys. 138, 154201-1–154201-7.
Galand, M. et al., 2010. Ionization sources in Titan's deep ionosphere. J. Geophys. Res. 115, A07312.
Galand, M., Coates, A.J., Cravens, T.E., Wahlund, J.-E., 2014. Titan's ionosphere. In: Mueller-Wodarg, I., Griffith, C., Lellouch, E., Cravens, T.E. (Eds.), Titan: Surface, Atmosphere, and Magnetosphere. Cambridge University Press (Cambridge Planetary Science Series), New York, pp. 376–418, ISBN: 0521199921.
Gronoff, G., Lilensten, J., Modolo, R., 2009. Ionization processes in the atmosphere of Titan. II. Electron precipitation along magnetic field lines. Astron. Astrophys. 506, 965–970.
Itikawa, Y., 2006. Cross sections for electron collisions with nitrogen molecules. J. Phys. Chem. Ref. Data 35, 31–53. http://dx.doi.org/10.1063/1.1937426.
Larsen, T.R. et al., 1972. Electron–ion and ion–ion reaction rate coefficients at low altitudes during a PCA event. J. Atmos. Terr. Phys. 34, 787–794.
Lavvas, P., Galand, M., Yelle, R.V., et al., 2011. Energy deposition and primary chemical products in Titan's upper atmosphere. Icarus 213, 233–251.
Lavvas, P., Yelle, R.V., Koskinen, T., et al., 2013. Aerosol growth in Titan's ionosphere. PNAS 110, 2729–2734.
Lewis, G.R. et al., 2008. Derivation of density and temperature from the Cassini–Huygens CAPS electron spectrometer. Planet. Space Sci. 56, 901–912.
Lewis, G.R. et al., 2010. The calibration of the Cassini–Huygens CAPS electron spectrometer. Planet. Space Sci. 58, 427–436.
Liu, X., Shemansky, D.E., 2006. Analysis of electron impact ionization properties of methane. J. Geophys. Res. 111, A04303.
Mandt, K.E. et al., 2012. Ion densities and composition of Titan's upper atmosphere derived from the Cassini Ion Neutral Mass Spectrometer: Analysis methods and comparison of measured ion densities to photochemical model simulations. J. Geophys. Res. 117, E10006.
Rebrion-Rowe, C. et al., 1998. The dissociative recombination of hydrocarbon ions. II. Alkene and alkyne derived species. J. Chem. Phys. 108, 7185–7189.
Richard, M.S., 2013. Plasma Interactions in Titan's Ionosphere, PhD Thesis, University of Kansas.
Robertson, I.P. et al., 2009. Structure of Titan's ionosphere. Model comparisons with Cassini data. Planet. Space Sci. 57, 1834–1846.
Shebanits, O. et al., 2013. Negative ion densities in the ionosphere of Titan – Cassini RPWS/LP results. Planet. Space Sci. 84, 153–162.
Snowden, D. et al., 2013. Auroral electron precipitation and flux tube erosion in Titan's upper atmosphere. Icarus 226, 186–204.
Vigren, E., Galand, M., Yelle, R.V., et al., 2013. On the thermal electron balance in Titan's sunlit upper atmosphere. Icarus 223, 234–251.
Vigren, E., Galand, M., Shebanits, O., et al., 2014. Increasing positive ion number densities below the peak of ion-electron pair formation in Titan's ionosphere. Astrophys. J. 786, 69.
Vuitton, V., Yelle, R.V., McEwan, M.J., 2007. Ion chemistry and N-containing molecules in Titan's upper atmosphere. Icarus 191, 722–742.
Vuitton, V. et al., 2009. Negative ion chemistry in Titan's upper atmosphere. Planet. Space Sci. 57, 1558–1572.
Wahlund, J.-E. et al., 2009. On the amount of heavy molecular ions in Titan's ionosphere. Planet. Space Sci. 57, 1857–1865.
Waite Jr., J.H. et al., 2007. The process of tholin formation in Titan's upper atmosphere. Science 316, 870–875.
Wellbrock, A., Coates, A.J., Sillanpää, I., et al., 2012. Cassini observations of ionospheric photoelectrons at large distances from Titan: Implications for Titan's exospheric environment and magnetic tail. J. Geophys. Res. 117, A03216.
Wellbrock, A., Coates, A.J., Jones, G.H., Lewis, G.R., Waite, J.H., 2013. Cassini CAPS–ELS observations of negative ions in Titan's ionosphere: Trends of density with altitude. Geophys. Res. Lett. 40, 4481–4485.
Westlake, J.H. et al., 2012. Titan's ionospheric composition and structure: Photochemical modeling of Cassini INMS data. J. Geophys. Res. 117, E01003.
Woods, T.N. et al., 2005. Solar EUV experiment: Mission overview and first results. J. Geophys. Res. 110, A01312.